A Method for Optimizing the Base Position of Mobile Painting Manipulators

Shunan Ren, Ying Xie, Xiangdong Yang, Jing Xu, *Member, IEEE*, Guolei Wang, and Ken Chen, *Member, IEEE*

***Abstract*— This paper presents an algorithm to optimize the base position of a mobile manipulator to meet the requirements of local painting tasks. Considering the physical limits and singularity of the manipulator, the feasible base positions are first discretely calculated with the given poses of the end effector by inverse kinematics. Then, the joint-level performance criteria are proposed with respect to the requirements of the painting process. The weight coefficients are also determined by the critic method to balance the contribution of every criterion. Thus, the globally near-optimal base position is selected by sorting all feasible positions according to the evaluation criteria. The experimental results show that the planning result is well executed and has an acceptable computation time, thus demonstrating that the algorithm is both practical and effective compared with previous methods.**

***Note to Practitioners*—Finding a proper base position is pivotal for achieving automatic offline planning for a manipulator mounted on a mobile platform. We present an algorithm that leads to an appropriate base position for the manipulator by which the manipulator could reach all the target points with specific orientations and keep a stable velocity of the end effector. This will greatly facilitate the offline planning for mobile manipulator systems such as the painting system implemented in this paper. With no need to manually participate in the algorithm implementation, operators can simply import the path-point data and obtain the optimized base position. The experimental results presented in this paper are encouraging in that the velocity of the end effector is more stable and the planning efficiency is highly increased.**

***Index Terms*— Base position, mobile manipulator, offline planning, optimization method, spray painting.**

I. Introduction

MOBILE manipulators are employed to execute a wide range of painting tasks and have a mechanical structure referred to as repetitive workspace robots [1], in which the end effector can reach every target point on large compound surfaces. It is important to determine a proper base position for the manipulator so that the manipulator can exhibit its best reachability and dexterity. However, it is difficult for workers to determine the base position from which the manipulator can reach all the path points with a realistic process velocity. Therefore, it is meaningful to develop an optimization method to determine the base position automatically for large-part painting or similar applications.

Manuscript received November 11, 2015; revised June 23, 2016; accepted September 1, 2016. Date of publication October 10, 2016; date of current version January 4, 2017. This paper was recommended for publication by Associate Editor T. Bretl and Editor M. Wang upon evaluation of the reviewers' comments. This work was supported by the National Natural Science Foundation of China under Grant 61403226.

S. Ren is with the Institute of Automation, Chinese Academy of Sciences, Beijing 100190, China (e-mail: renshunan@gmail.com).

Y. Xie is with AVIC Chengdu Aircraft Industrial (Group) Company, Ltd., Chengdu 610092, China (e-mail: xmany@126.com).

X. Yang, J. Xu, G. Wang, and K. Chen are with the Department of Mechanical Engineering, Tsinghua University, Beijing 100084, China (e-mail: yangxd@tsinghua.edu.cn; jingxu@tsinghua.edu.cn; wangguolei@mail.tsinghua.edu.cn; kenchen@tsinghua.edu.cn).

Digital Object Identifier 10.1109/TASE.2016.2612694

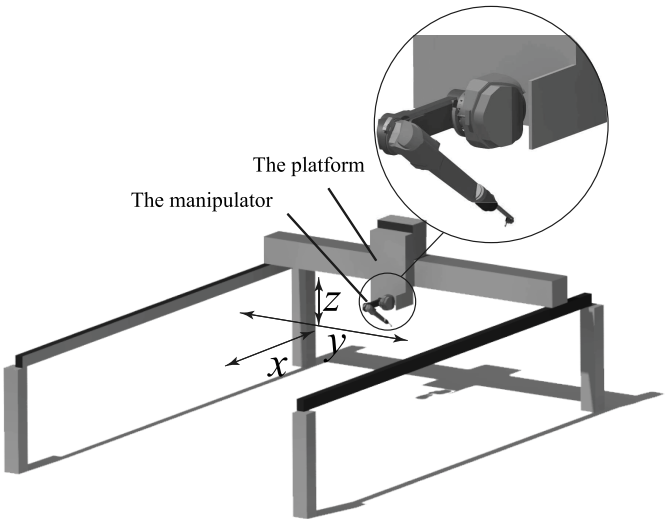

Fig. 1. Equipment implemented in this paper. The manipulator is mounted on a 3-D rail system.

Some manipulators are mounted on vehicles in [2] while others may be mounted on rail systems, as shown in Fig. 1. Robot arms installed on mobile platforms clearly have both the flexibility of the manipulator and the mobility that general industrial manipulators lack. These mobile manipulators are designed for dull, monotonous, dirty, and dangerous work [3], [4]. To achieve the desired level of performance, motion planning for mobile manipulators has been studied for several years according to the specific application. When the goal is pick-and-place or trajectory tracking, mobile manipulators are commonly viewed as integrated manipulators with redundant freedom. Carriker *et al.* [5] transformed the process of motion planning into an optimization problem that considered both the base position and the manipulator joint angles separately. A near-optimal result was obtained by simulated annealing according to the pose, force, and moment of the end effector. Zeghloul and Pamanes-Garcia [6] presented a method for determining the location of the manipulator with several constraints but did not provide the optimal algorithm. Yamamoto and Yun [7] proposed a control algorithm that first measured the joint angles and then performed the motion planning of the platform, keeping the manipulator within a preferred manipulability. Gardner and Velinsky [8] added joint velocities to the definition of manipulability, through which they analyzed the kinematic performance of the overall mobile manipulator system. Mitsi *et al.* [9] viewed the base location as a variable, and employed a hybrid heuristic optimization method with the genetic, quasi-Newton algorithm and the constraints handling method to obtain the global optimal solution. Nektarios and Aspragathos [10] optimized the placement of the manipulator to obtain the desired velocity performance. They proposed the concept of approximation of the minimum manipulator velocity ratio to represent the worst kinematic abilities and used a genetic algorithm to obtain an optimal or suboptimal solution. Galicki [11] proposed a control scheme based on Lyapunov stability theory, which helped implement online trajectory tracking. Alipour and Moosavian [12] presented a motion planning method to maintain

stability when the mobile manipulator executed heavy lifting tasks. Xiao and Zhang [13] also proposed a repetitive motion scheme that considered physical limits. Synodinos *et al.* [14] developed an effective fuzzy system to approximately describe the manipulability and condition number of a mobile manipulator that was less time-consuming and very useful for real-time motion planning.

These studies provide beneficial explorations into motion planning, including the manipulator itself and the mobile platform. Several optimization methods have been investigated on a range of objectives including cycle time, manipulability, condition number, stability, and dynamic performance, among others. Nevertheless, a couple of problems still remain. When the manipulator is heavy, coordinating its motion with the platform will result in the end effector being less stable. Thus, the system cannot be considered to be a redundant robot. Meanwhile, most previous studies have focused on the placement of manipulators utilized for assembly or transportation work, in which, characteristically, there are only a few path points along which to track. However, as the number of the path points increases, the time cost of the calculation will rapidly increase when using the aforementioned methods. Furthermore, some heuristic algorithms rely on finding configuration settings through trial and error; however, doing so is complex and the result may be locally optimal—which cannot satisfy the requirements of automatic planning.

The remainder of this paper is organized as follows. In Section II, the problem is illustrated in detail. In Section III, we introduce a series of coordinate systems to facilitate the description. In Section IV, we address the base position optimization problem and present a practical algorithm. In Section V, the algorithm is validated through experiments and the results are discussed. Finally, conclusions are provided in Section VI.

II. Problem Statement

The workspace reachable by the manipulator is limited. Therefore, either larger or additional manipulators are required to cover an entire working area that is both expensive and impractical. An economical solution to this problem is to separate the working area into smaller areas, each of which can be completely contained in the workspace of a single manipulator. The manipulator simply needs to work within these partitions, and it is shifted from one base position to another by the mobile platform.

In our implementation, the action objects are multitype parts and sometimes change. Therefore, we focus primarily on the strategy for determining an optimized base position to reduce the planning time. A standard industrial painting manipulator (ABB Flexpainter IRB 5500 series) is mounted on a mobile orthogonal coordinative machine, as shown in Fig. 1. Due to the weight of the manipulator (approximately 600 kg), the manipulator executes the painting task independently after the platform moves to a given position and stops. This helps ensure structural stiffness and coating quality in comparison with the operation mode in the existing automatic painting system [15], which does not emphasize the stability of the end effector.

To satisfy the specific requirements of the painting process and guarantee uniform paint coating, it is generally acknowledged that the end effector must meet the following conditions during work.

1) The end effector should be able to reach every target path point on the task trajectory.
2) The velocity of the end effector should be maintained.

The base position of the manipulator clearly has a significant impact on the above factors. An appropriate base position should be determined that satisfies both the requirements.

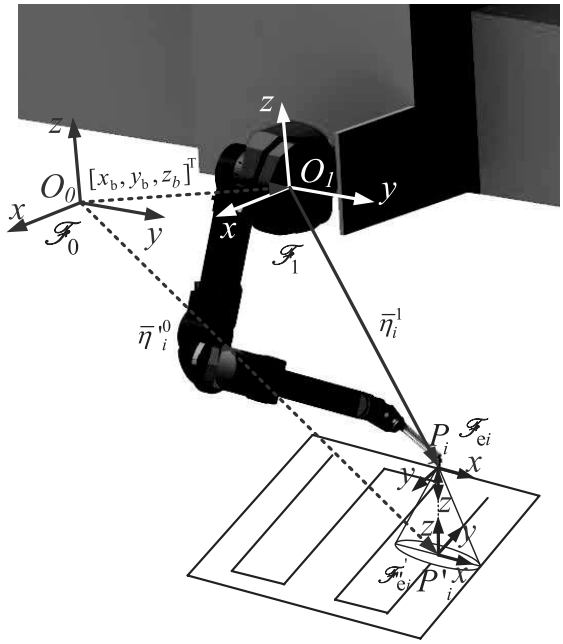

Fig. 2. Coordinate frames for the painting system: $\mathcal{F}_0$ is the global frame, $\mathcal{F}_1$ is the local frame of the manipulator, and $\mathcal{F}'_{ei}$ and $\mathcal{F}_{ei}$ are local frames that describe the path points on the surface and the trajectory of the end effector, respectively.

III. Preliminary Work

Before implementing the algorithm to optimize the base position, the positions and orientations of the end effector should be identified. To clearly illustrate this information, a couple of coordinate systems are first formulated. Then, a transformation from the trajectory on the surface to the poses of the end effector is introduced.

A. Definition of Coordinate Systems

All the parts including the painting manipulator, base platform, and surfaces to be painted are modeled using a global coordinate frame denoted as $\mathcal{F}_0$. Then, we attach an inertial reference frame $\mathcal{F}_1$ to the base of the manipulator. The directions of the axes are the same as in the global coordinate system.

When the paint gun operates, the spray shape is considered to be an elliptical cone, which is widely adopted as the deposition model in the painting process. The central bottoms of these spray cones are on the planned trajectory on the surface, denoted as P'_i $(i = 1, 2, \ldots, N)$. N is the total number of trajectory points on the surface. Thus the path points on the surface determine not only the location but also the orientation of the spray cone. Then, the path points P_i of the end effector can be obtained, which are shifted from P'_i along the normal vectors by d_{gun}. The translational distance d_{gun} is determined by the process requirements.

To facilitate this description, two local inertial frames $\mathcal{F}'_{ei}$ and $\mathcal{F}_{ei}$ $(i = 1, 2, \ldots, N)$ are assigned for every path point on the surface and the trajectory of the end effector ("e" denotes the end effector). The original points are at P'_i and P_i, respectively. For $\mathcal{F}'_{ei}$, the z-axis is aligned with the normal direction of the corresponding point P'_i and the x-axis is aligned along the long axis of the elliptical section in the spray cone. For $\mathcal{F}_{ei}$, the x-axis is aligned with the x-axis of $\mathcal{F}'_{ei}$, whereas the y- and z-axes are opposite to those of $\mathcal{F}'_{ei}$. All the determined local frames are shown in Fig. 2.

B. Pose Calculation of the Paint Gun Orientation

We now provide a method for calculating the position and orientation of the end effector according to path points on the surface.

Some studies of how to perform trajectory planning for painting manipulators have been performed. An equidistant raster trajectory is widely recognized as the preferred method [16]–[18]. In our practical work, we utilize the advanced machining tool in CATIA to generate the desired isometric trajectory on the surface, as shown in Fig. 2.

Thus, P'_i is the ith path point of the trajectory on the surface and the vector representation is

$$\bar{\eta}'^0_i = \left[x'^0_i, y'^0_i, z'^0_i, \alpha'^0_i, \beta'^0_i, \gamma'^0_i\right]^{\mathrm{T}} \tag{1}$$

where $\bar{\eta}'^0_i$ describes the relationship between the frames $\mathcal{F}'_{ei}$ and $\mathcal{F}_0$. x'^0_i, y'^0_i, and z'^0_i are the coordinates of P'^0_i under $\mathcal{F}_0$. Here, α'^0_i, β'^0_i, and γ'^0_i are, respectively, the yaw, pitch, and roll angles of frame $\mathcal{F}'_{ei}$ under $\mathcal{F}_0$.

According to the formulation rules, we can also obtain the position and orientation of the end effector under $\mathcal{F}_1$, expressed as $\bar{\eta}^1_i$

$$\bar{\eta}^1_i = \left[x^1_i, y^1_i, z^1_i, \alpha^1_i, \beta^1_i, \gamma_i{}^1\right]^{\mathrm{T}} \tag{2}$$

in which

$$\begin{cases} x^1_i = x'^0_i - x_b + d_{\mathrm{gun}} \\ \qquad \times \left(\cos\alpha'^0_i \sin\beta'^0_i \cos\gamma'^0_i + \sin\alpha'^0_i \sin\gamma'^0_i\right) \\ y^1_i = y'^0_i - y_b + d_{\mathrm{gun}} \\ \qquad \times \left(\cos\alpha'^0_i \sin\beta'^0_i \sin\gamma'^0_i - \sin\alpha'^0_i \cos\gamma'^0_i\right) \\ z^1_i = z'^0_i - z_b + d_{\mathrm{gun}} \cos\alpha'^0_i \cos\beta'^0_i \\ \alpha^1_i = \alpha'^0_i - \pi \\ \beta^1_i = \beta'^0_i \\ \gamma^1_i = \gamma'^0_i \end{cases} \tag{3}$$

where x_b, y_b, and z_b are the coordinates of the base position under $\mathcal{F}_0$, x^1_i, y^1_i, and z^1_i are the coordinates of P_i under $\mathcal{F}_1$, and α^1_i, β^1_i, and γ^1_i are the yaw, pitch, and roll angles, respectively.

IV. Two-Step Algorithm of Determining the Base Position

Due to the flexibility of the manipulator, it is not cost-effective to find the exact optimal base position given the high price of considerable planning time, particularly when the base position needs to be changed frequently when painting large parts. In this section, we provide a method for determining the globally near-optimal base position. In fact, some strong constraints exist when the manipulator is utilized to paint. For example, the joints should be far away from the singular position and not exceed the physical limits. When this occurs, the manipulator will stop, leading to a detrimental impact on the coating quality. Thus, a two-step algorithm is proposed here that first finds the feasible base position globally and, then, employs some criteria to evaluate the feasible base positions from which the best one is selected.

A. Acquiring Feasible Base Positions

From (3), the path points of the paint gun, $\bar{\eta}^1_i$ are obtained through $\bar{\eta}'^0_i$. Then, we denote the central point of the surface segment as P'_{c}, which is the projection of the orthocenter. The normal vector at P'_{c} is denoted as $\bar{n}' = [n'_x, n'_y, n'_z]^{\mathrm{T}}$ under $\mathcal{F}_0$.

Next, a series of discrete positions that are in the upper space of the surface are generated to obtain feasible base positions. To facilitate describing these discrete positions, an inverted cone area is formed that pivots around $\bar{n}$ at P_{c} as shown in Fig. 3. P_{c} is d_{gun} from P'_{c} along $\bar{n}'$. Additionally, $\bar{n}$ is identical to $\bar{n}'$, expressed under $\mathcal{F}_0$.

To reduce the computation time, we limit the search range inside an area constrained by the minimum and maximum radii ($r_{\min}$ and $r_{\max}$, respectively) that the manipulator can reach. Thus, we denote

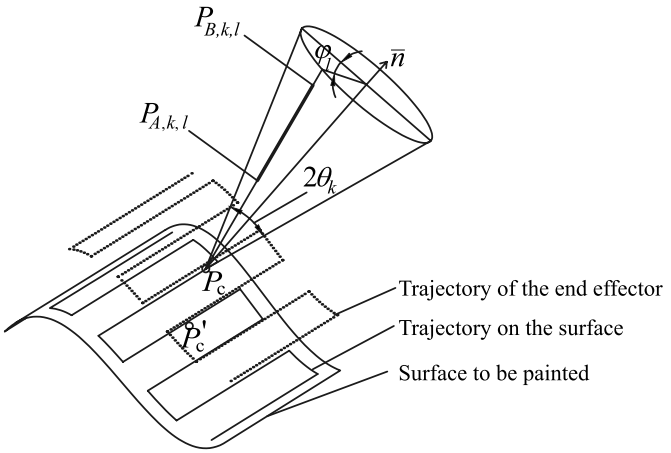

Fig. 3. Upper space of the target surface is discretized by a cone [19].

the points on the cone surface that are $r_{\min}$ and $r_{\max}$ away from the peak point as $P_{A,k,l}$ and $P_{B,k,l}$, respectively. Then, the discrete base position is

$$P_{k,l,q} = P_{A,k,l} + \frac{q}{Q}(P_{B,k,l} - P_{A,k,l}) \tag{4}$$

in which $q = 0, 1, \ldots, Q$ where $P_{A,k,l}$ and $P_{B,k,l}$ can be calculated by θ_k and φ_l, where

$$\theta_k = k\frac{\pi}{2K}, \quad k = 0, 1, \ldots, K \tag{5}$$

and

$$\varphi_l = l\frac{2\pi}{L}, \quad l = 0, \ldots, L-1. \tag{6}$$

Here, θ_k is half the point angle of the search cone area and φ_l is the rotation angle about axis $\bar{n}$.

We place the base of the manipulator at $P_{k,l,q}$ with k, l, and q in increasing order if it is within the motion range of the platform. Then, the vectors $\bar{\eta}^1_i$ of the path points P_i are imported to perform the inverse kinematics calculation. The analytical solution of the inverse kinematics equation for an ABB IRB 5500 does not exist because of its nonspherical wrist and extra joint. Thus, a numerical solution was previously presented in [20], which was shown to be reliable and highly effective in practice.

During the calculation process, it is necessary to consider the kinematic singularities of the manipulator. In [21], singularity is classified into three cases: elbow singularity, shoulder singularity, and wrist singularity. For the specific manipulator in this paper, it falls into the wrist singularity when joint 5 is near zero, which makes the axes of joints 4 and 6 collinear. Meanwhile, no joint can be allowed to approach its physical limit.

To quickly obtain the feasible base positions, we define the point $P_{k,l,q}$ as a feasible base position if it satisfies the following conditions.

1) For every pose described in the sequence $\bar{\eta}^1_i$, the inverse kinematic solution $\bar{\theta}_{i,k,l,q}$ exists. In addition, the solution should not exceed the joint motion range of the manipulator, namely, $\bar{\theta}_{i,k,l,q} \in [\bar{\theta}_{\min}, \bar{\theta}_{\max}]$.
2) During the painting task, all values of joint 5 should be out of the range $[-10°, 10°]$, which are empirical data from experiments.

The computation runs until all the discrete points on the cone's surface are traversed with increasing k, l, and q.

B. Acquiring the Near-Optimal Base Position

As expected, there are typically numerous feasible base positions for a surface segment. In this section, an evaluation index is established to select the best position from the feasible ones.

Obviously, the most preferable base position is one in which the manipulator could maintain a more flexible configuration. In the past, manipulability has played an important role in evaluating this property. Manipulability is defined as the ability of the manipulator to move toward all directions [22] and is evaluated using Jacobian-based indices [23], [24]. These metrics describe the overall kinematic behavior, but due to the painting manipulator's predefined motion, it is a waste of workspace to consider the omnidirectional moving ability. Therefore, we proposed some joint-level criteria to evaluate the feasible base positions based on the inverse kinematic solutions.

We first let ξ_1 describe the reachability of the manipulator. Base positions in which the joint configurations concentrate in the intermediate region of the motion range are preferable. Due to the sufficiently wide motion ranges of joints 4–6, we simply focus on the first three joints here

$$\xi_1 = \left\{ \frac{1}{3N} \sum_{i=1}^{N} \left[\left(\frac{|\theta_{i,1} - \theta_{\mathrm{m},1}|}{\theta_{1,\max}} \right)^4 + \left(\frac{|\theta_{i,2} - \theta_{\mathrm{m},2}|}{\theta_{2,\max}} \right)^4 + \left(\frac{|\theta_{i,3} - \theta_{\mathrm{m},3}|}{\theta_{3,\max}} \right)^4 \right] \right\}^{\frac{1}{4}}. \tag{7}$$

In the preceding equation, N is the number of path points, $\theta_{i,j}$ is the configuration of the jth joint corresponding to the ith path point, and $\theta_{m,j}$ is the middle value of the jth joint's motion range. The relatively high index guarantees that a significant impact on the value occurs when the joints approach to their physical limits according to [25].

Second, ξ_2 is introduced to reflect the change in the joints corresponding to the adjacent path points. Less change means a lower driver load and a more stable velocity of the end effector. Likewise, we do not consider joints 4–6, which can support a rather high rate

$$\xi_2 = \left\{ \frac{1}{3(N-1)} \sum_{i=1}^{N-1} \left[\left(\frac{\theta_{i+1,1} - \theta_{i,1}}{\theta_{1,\max}} \right)^2 + \left(\frac{\theta_{i+1,2} - \theta_{i,2}}{\theta_{2,\max}} \right)^2 + \left(\frac{\theta_{i+1,3} - \theta_{i,3}}{\theta_{3,\max}} \right)^2 \right] \right\}^{\frac{1}{2}}. \tag{8}$$

Finally, an item is also added in ξ_3 to consider the relationship between joints 4 and 6. This is particularly important for the painting manipulator due to the need to avoid twisting the painting hoses

$$\xi_3 = \left\{ \frac{1}{N} \sum_{i=1}^{N} \left(\frac{\theta_{i,4} + \theta_{i,6}}{\theta_{4-6}} \right)^4 \right\}^{\frac{1}{4}}. \tag{9}$$

The index is set as 4 to guarantee that the value changes significantly when the coupled joints 4 and 6 approach $\pm 2\pi$. Let $\theta_{4-6} = 4\pi$, which is the motion range of the coupled joints 4 and 6 according to the manuals of the manipulator.

After the evaluation criteria have been established, the optimization objective is to select the position that minimizes $\xi_t (t = 1, 2, 3)$. It is evident that the three indices cannot be compared because of their different magnitudes. To overcome this problem, a normalized index was designed in [6], and it is expressed as follows:

$$\xi_t^* = \frac{\xi_t}{\max(\xi_t)} \tag{10}$$

where $\max(\xi_t)$ is the maximum value that ξ_t can reach among the results of all feasible base positions. Therefore, the ranges of ξ_t^* are unified to [0, 1] without losing any information.

It is more important that the weight coefficients are also required to balance the contribution of those indices because the three indices generally cannot reach the minimum value simultaneously. The critic method proposed in [26] is employed to determine those coefficients here. The weight values can be obtained through the following process:

$$C_t = \sigma_t \sum_{s=1}^{3} (1 - r_{st}) \quad t = 1, 2, 3 \tag{11}$$

$$w_t = \frac{C_t}{\sum_{t=1}^{3} C_t} \tag{12}$$

where C_t represents the amount of information included in the tth criterion. It considers both the alternatives' performances and the conflicts between every two criteria. σ_t is the standard deviation of the tth criterion's value representing its alternatives' performance; r_{st} is the correlation coefficient of the sth and tth criteria representing the conflict between them; and w_t is the weight for the tth criterion. For further details, the readers are referred to [26].

Thus, the final evaluation criterion is established as follows:

$$\xi^* = w_1 \xi_1^* + w_2 \xi_2^* + w_3 \xi_3^*. \tag{13}$$

After testing every feasible base position by ξ^*, the point position with the smallest value is finally selected as the best base position. Because the initial imported base position is discrete over the space, the result is globally near optimal. When K, L, and Q are large enough, the result is near the optimal position, but only at the cost of considerably more computation time. The overall algorithm is described in the pseudocode as follows.

V. Experiment and Discussion

The planning algorithm is implemented in C++ for the first step and MATLAB for the second step. The result is tested through experiments.

Because the presented algorithm is related only to the property of the surface containing the size and orientation, we choose four types of freeform surfaces facing different directions and two sizes as the objects, based on practical work situations. The experimental environment is shown in Fig. 4 in which (a)–(c) are approximately 1.8 m × 1.8 m with different poses, while Fig. 4(d) is 3.5 m × 3.5 m.

The painting trajectory can be generated by the CAM module of CATIA and transformed into the path points of the end effector. From the documentation, the reachable range of the manipulator is acquired as $r_{\min} = 600$ mm and $r_{\max} = 3000$ mm. To reduce the time cost and guarantee the density of the calculation, we determine the following parameters for the searching cone through several experiments: $K = 10$, $L = 20$, and $Q = 20$. Using these parameter values, the distance between two adjacent points is sufficiently small, and we obtain a total of 4620 base positions.

The algorithm is performed on a PC with an Intel i7 CPU and 8 GB of memory. The calculation time is acceptable. The total calculation time is 7 min for 67 path points, which is considerably less than the 23 min required for seven path points in [6] or the 16 min required for nine path points in [9], as shown in Table I. There is no feasible base position in scenario 4 in which the objective surface is too large. The property of the best base position is illustrated in Table II.

Afterward, the corresponding best base positions are substituted into the manipulator to conduct the experiment. The position of the

Algorithm 1: Planning the Base Position for a Mobile Manipulator

Input: The path points of the trajectory on the surface $\bar{\eta}_i'^0, i = 1, 2, \ldots, N$

Output: The best base position x^0, y^0, z^0

for *every* $P_{k,l,q}$ *in the motion range of the platform* **do**
  Let x_b, y_b, z_b represent $P_{k,l,q}$, FeasibleFlag=false;
  for $i = 1,2,\ldots,N$ **do**
    Compute $\bar{\eta}_i^1$; Refer to (2).
    Compute the inverse kinematics solution $\bar{\theta}_{i,k,l,q}$ for $\bar{\eta}_i^1$; Refer to [20].
    if $\bar{\theta}_{i,k,l,q} \notin [\bar{\theta}_{\min}, \bar{\theta}_{\max}]$ *or* $\theta_{i,k,l,q,5} \in [-10°, 10°]$ **then**
      FeasibleFlag=false;
      break;
    end
    FeasibleFlag=true;
  end
  if *FeasibleFlag==true* **then**
    Mark x_b, y_b, z_b as a feasible base position;
  end
end
for *every feasible base position* **do**
  Compute evaluation criterion ξ^*; Refer to (13).
end
Return the best base position as x^0, y^0, z^0 with the least value of ξ^*;

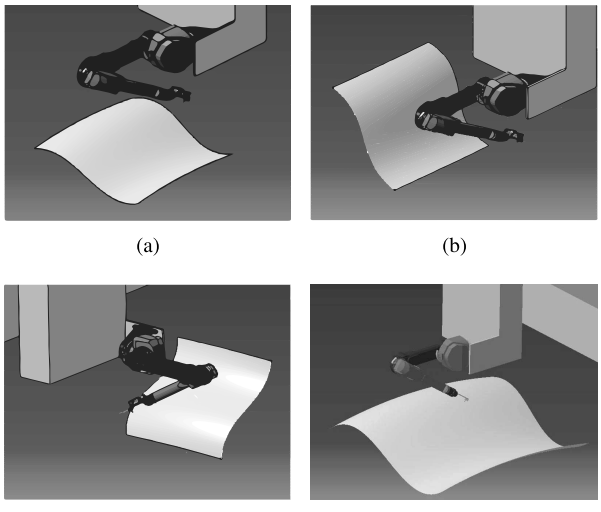

Fig. 4. Four scenarios to be tested. (a) Surface is nearly horizontal. (b) Surface leans to the right. (c) Surface leans to the left. (d) Larger surface is nearly horizontal.

end effector is measured using a Leica AT901 laser tracker with a spherical reflector at the position of the paint gun. The sampling mode is continuous, with an interval of 100 ms. The velocity can be obtained by dividing the distance by the time.

Fig. 5 presents a comparison between ξ^* and the end effector's velocity between the base positions with and without optimization. We previously defined the base position by translating P_c' along the normal vector by a fixed distance (2500 mm). There are only two groups of comparisons, scenarios 1 and 3, because the base position generated by the original method fails for scenario 2. Although the average velocity v_E of the end effector is nearly equivalent, the standard deviation σ_v of the end effector's velocity after optimization is smaller, which means a more stable velocity and, consequently, better coating quality.

The experimental results show that the algorithm proposed in this paper is both practical and effective. Although not perfectly optimal, it is still globally near optimal to help the end effector maintain a stable velocity. Thus, it is sufficient to improve the offline planning efficiency while still ensuring a satisfactory painting quality.

Naturally, the algorithm cannot provide a proper base position when the size of the surface is too large as in scenario 4. In that scenario, the working area is so large that the end effector cannot reach every path point. The solution is to reduce the surface area, replan the trajectory and, then, reexecute the algorithm. The manipulator generally has its own proper manipulation range empirically, for example, an area of 2 m × 2 m for the ABB IRB 5500.

TABLE I
FEASIBLE BASE POSITIONS

Scenario	Number of Path Points	Feasible Base Positions	Time Cost(m)
1	67	788	7.0
2	67	219	7.0
3	67	583	7.1
4	131	0	13.3
[6]	7	—	23
[9]	9	—	16

TABLE II
OPTIMIZATION RESULT

Scenario	Min ξ^*	Weights $w_1\backslash w_2\backslash w_3$	Corresponding $\xi_1^*\backslash\xi_2^*\backslash\xi_3^*$	Max $\xi_1\backslash\xi_2\backslash\xi_3$
1	0.43	0.29\0.16\0.55	0.43\0.50\0.41	0.32\0.06\0.39
2	0.54	0.23\0.20\0.57	0.69\0.58\0.46	0.31\0.05\0.35
3	0.42	0.28\0.24\0.48	0.57\0.54\0.27	0.35\0.06\0.67
4	—	—	—	—

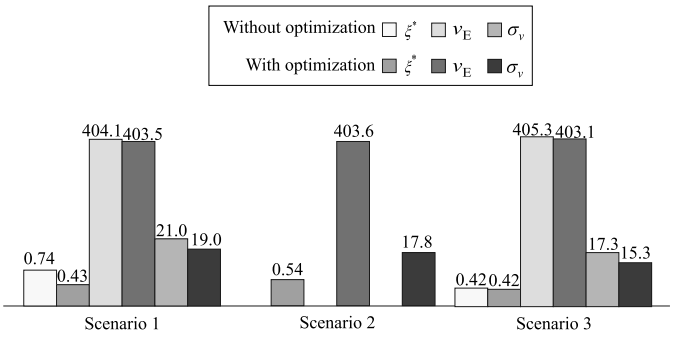

Fig. 5. Comparison between the base positions with and without optimization: ξ^* is the evaluation criterion, v_E is the average velocity of the end effector, and σ_v is the standard deviation of the end effector's velocity.

VI. CONCLUSION

In this paper, we formulate a method for base position planning to plan the base position for a mobile painting manipulator. It is difficult to manually determine a proper base position for the manipulator that satisfies the requirements of painting processes. Therefore, we present a two-step search algorithm for a nearly optimal base position.

An experiment is performed, and the result shows that the proposed algorithm allows a larger local painting area and supports a more stable end-effector velocity during the painting process. The implementation of the algorithm also significantly decreases the offline planning time compared with other algorithms. It is suggested that proper surface segments should be prepared in advance to improve the planning process.

REFERENCES

[1] S. Seriani, P. Gallina, and A. Gasparetto, "A performance index for planar repetitive workspace robots," *ASME J. Mech. Robot.*, vol. 6, no. 3, p. 031005, Apr. 2014.

[2] P. J. From, J. T. Gravdahl, and K. Y. Pettersen, *Vehicle-Manipulator Systems*. London, U.K.: Springer, 2014.

[3] P. J. From, V. Duindam, K. Y. Pettersen, J. T. Gravdahl, and S. Sastry, "Singularity-free dynamic equations of vehicle–manipulator systems," *Simul. Model. Pract. Theory*, vol. 18, no. 6, pp. 712–731, Jun. 2010.

[4] M. Hvilshøj, S. Bøgh, O. S. Nielsen, and O. Madsen,, "Autonomous industrial mobile manipulation (AIMM): Past, present and future," *Ind. Robot Int. J.*, vol. 39, no. 2, pp. 120–135, 2012.

[5] W. F. Carriker, P. K. Khosla, and B. H. Krogh, "Path planning for mobile manipulators for multiple task execution," *IEEE Trans. Robot. Autom.*, vol. 7, no. 3, pp. 403–408, Jun. 1991.

[6] S. Zeghloul and J. Pamanes-Garcia, "Multi-criteria optimal placement of robots in constrained environments," *Robotica*, vol. 11, no. 2, pp. 105–110, Mar. 1993.

[7] Y. Yamamoto and X. Yun, "Coordinating locomotion and manipulation of a mobile manipulator," *IEEE Trans. Autom. Control*, vol. 39, no. 6, pp. 1326–1332, Jun. 1994.

[8] J. F. Gardner and S. A. Velinsky, "Kinematics of mobile manipulators and implications for design," *J. Robot. Syst.*, vol. 17, no. 6, pp. 309–320, Jun. 2000.

[9] S. Mitsi, K.-D. Bouzakis, D. Sagris, and G. Mansour, "Determination of optimum robot base location considering discrete end-effector positions by means of hybrid genetic algorithm," *Robot. Comput.-Integr. Manuf.*, vol. 24, no. 1, pp. 50–59, Feb. 2008.

[10] A. Nektarios and N. A. Aspragathos, "Optimal location of a general position and orientation end-effector's path relative to manipulator's base, considering velocity performance," *Robot. Comput.-Integr. Manuf.*, vol. 26, no. 2, pp. 162–173, Apr. 2010.

[11] M. Galicki, "Task space control of mobile manipulators," *Robotica*, vol. 29, no. 2, pp. 221–232, Mar. 2011.

[12] K. Alipour and S. A. A. Moosavian, "Dynamically stable motion planning of wheeled robots for heavy object manipulation," *Adv. Robot.*, vol. 29, no. 8, pp. 545–560, 2015.

[13] L. Xiao and Y. Zhang, "A new performance index for the repetitive motion of mobile manipulators," *IEEE Trans. Cybern.*, vol. 44, no. 2, pp. 280–292, Feb. 2014.

[14] A. Synodinos, V. C. Moulianitis, and N. Aspragathos, "A fuzzy approximation to dexterity measures of mobile manipulators," *Adv. Robot.*, vol. 29, no. 2, pp. 753–769, 2015.

[15] N. A. Seegmiller, J. A. Bailiff, and R. K. Franks, "Precision robotic coating application and thickness control optimization for F-35 final finishes," *SAE Int. J. Aerosp*, vol. 2, no. 1, pp. 284–290, 2010.

[16] W. Sheng, H. Chen, N. Xi, and Y. Chen, "Tool path planning for compound surfaces in spray forming processes," *IEEE Trans. Autom. Sci. Eng.*, vol. 2, no. 3, pp. 240–249, Jul. 2005.

[17] M. A. Arikan and T. Balkan, "Process simulation and paint thickness measurement for robotic spray painting," *CIRP Ann.-Manuf. Techn.*, vol. 50, no. 1, pp. 291–294, 2001.

[18] P. N. Atkar, A. Greenfield, D. C. Conner, H. Choset, and A. A. Rizzi, "Uniform coverage of automotive surface patches," *Int. J. Robot. Res.*, vol. 24, no. 11, pp. 883–898, Nov. 2005.

[19] S. Ren, Y. Xie, Z. Liu, G. Wang, X. Yang, and K. Chen, "Base station searching for manipulators with huge objective workpieces," in *Proc. IEEE Int. Conf. Cyber Technol. Autom., Control, Intell. Syst. (CYBER)*, Jun. 2015, pp. 252–257.

[20] L. Wu, X. D. Yang, D. J. Miao, Y. Xie, and K. Chen, "Inverse kinematics of a class of 7R 6-DOF robots with non-spherical wrist," in *Proc. IEEE Int. Conf. Mecha. Autom.*, Aug. 2013, pp. 69–74.

[21] M. Hayes, M. Husty, and P. Zsombor-Murray, "Singular configurations of wrist-partitioned 6R serial robots: A geometric perspective for users," *Trans. Can. Soc. Mech. Eng.*, vol. 26, no. 1, pp. 41–55, 2002.

[22] R. M. Murray, R. M. Murray, Z. Li, Z. Li, and S. S. Sastry, *A Mathematical Introduction to Robotic Manipulation*. Boca Raton, FL, USA: CRC Press, 1994.

[23] J. K. Salisbury and J. J. Craig, "Articulated hands force control and kinematic issues," *Int. J. Robot. Res.*, vol. 1, no. 1, pp. 4–17, 1982.

[24] T. Yoshikawa, "Manipulability of robotic mechanisms," *Int. J. Robot. Res.*, vol. 4, no. 2, pp. 3–9, 1985.

[25] C. D. Cocca and D. Tesar, "Failure recovery in redundant serial manipulators," Ph.D. dissertation, Dept. Mech. Eng., Univ. Texas Austin, Austin, TX, USA, 2000.

[26] D. Diakoulaki, G. Mavrotas, and L. Papayannakis, "Determining objective weights in multiple criteria problems: The critic method," *Comput. Oper. Res.*, vol. 22, no. 7, pp. 763–770, Aug. 1995.